

Orbital ordering and unfrustrated $(\pi, 0)$ magnetism from degenerate double exchange in the iron pnictides

Weicheng Lv, Frank Krüger, and Philip Phillips

Department of Physics, University of Illinois, 1110 West Green Street, Urbana, Illinois 61801, USA

(Dated: May 31, 2018)

The magnetic excitations of the iron pnictides are explained within a degenerate double-exchange model. The local-moment spins are coupled by superexchanges J_1 and J_2 between nearest and next-nearest neighbors, respectively, and interact with the itinerant electrons of the degenerate d_{xz} and d_{yz} orbitals via a ferromagnetic Hund exchange. The latter stabilizes $(\pi, 0)$ stripe antiferromagnetism due to emergent ferro-orbital order and the resulting kinetic energy gain by hopping preferably along the ferromagnetic spin direction. Taking the quantum nature of the spins into account, we calculate the magnetic excitation spectra in the presence of both, super- and double-exchange. A dramatic increase of the spin-wave energies at the competing Néel ordering wave vector is found, in agreement with recent neutron scattering data. The spectra are fitted to a spin-only model with a strong spatial anisotropy and additional longer ranged couplings along the ferromagnetic chains. Over a realistic parameter range, the effective couplings along the chains are negative corresponding to unfrustrated stripe antiferromagnetism.

PACS numbers: 74.70.Xa, 75.25.Dk, 74.25.Ha, 71.10.Fd

I. INTRODUCTION

The discovery of superconductivity in the pnictides¹⁻⁶ with transition temperatures challenging those of single-layer, high- T_c cuprates, immediately raised the question of whether, despite all their differences, the two classes of materials share the same key mechanism for superconductivity.⁷⁻⁹ Arguably the most striking similarity is that superconductivity emerges upon doping antiferromagnetically ordered parent compounds. In the pnictides, however, the magnetic ordering is unusual, characterized by an antiferromagnetic arrangement of ferromagnetic chains, corresponding to an in-plane ordering wave vector $\mathbf{Q} = (\pi, 0)$.¹⁰⁻¹⁹ Whereas the pnictides are metallic, the parent cuprates are Mott insulators. The conductivities in the pnictides are typical of bad metals, suggesting that electronic correlations²⁰⁻²⁹ are crucial. By contrast, the local-density approximation seems to be adequate³⁰ to describe their band structure.

As a result of this dichotomy, both itinerant-magnetism³⁰⁻³⁸ and local-moment^{27-29,39-44} scenarios have been suggested to explain the unusual stripe antiferromagnetism. Although the former weak-coupling theories which attribute the magnetism to a spin-density-wave instability of a nested Fermi surface, can explain the magnetic low-energy excitations around the correct ordering wave vector, they fail to describe the spectra at higher energies which have been measured in great detail by inelastic neutron scattering.^{45,46} In particular, the itinerant scenarios can not explain the observed maximum of the dispersion at (π, π) but rather suggest that the excitations rapidly dissolve into a particle-hole continuum³⁷ which has not been found experimentally up to energies of 200meV. So far, a consistent description of the excitations over the entire energy range has been obtained only by using suitably parametrized Heisenberg models.

Because of the positions of the arsenic ions above

or below the iron plaquettes, such a spin-only model is expected to be strongly frustrated with comparable, antiferromagnetic superexchanges J_1 and J_2 between nearest and next-nearest neighbors. In this regime, the model indeed exhibits long-range stripe-antiferromagnetic order,⁴⁷⁻⁴⁹ and the strong frustration and proximity to a continuous magnetic phase transition might explain why the observed magnetic moments are relatively small.^{27,42} Interestingly, the neutron-scattering experiments tell a radically different story. The spin-wave velocities indicate that the exchange coupling along the ferromagnetic spin direction is much smaller than the one perpendicular to the chains,⁴⁵ $J_{1y} \ll J_{1x}$. More recently, it has been argued⁴⁶ that the observed maximum of the dispersion at (π, π) requires an even slightly ferromagnetic exchange $J_{1y} < 0$ corresponding to an unfrustrated spin model in contrast to early claims²⁷ of high frustration.

What might be the cause of such a strong spatial anisotropy? In fact, before the magnetic order sets in, a structural transition occurs at which the two in-plane lattice constants become inequivalent. The structural and magnetic transition are clearly separated in the so-called ‘1111 compounds’,¹⁰⁻¹³ whereas they occur at the same temperature in the ‘122 family’.¹⁴⁻¹⁷ However, inspecting the numbers, it appears that the orthorhombic lattice distortion is too small, by two orders of magnitude, to explain the magnetic anisotropy.⁴⁴

To this end, some have proposed^{40,50-52} that orbital-ordering physics of a similar kind as in the manganite transition-metal oxides not only provides a mechanism for the lattice distortion but more importantly explains the strong in-plane anisotropies. In particular, it has been argued⁴⁰ that due to an orbital degeneracy, the localized limit is described by a complicated spin-orbital superexchange (Kugel-Khomskii) model rather than by a Heisenberg Hamiltonian. Further, it was shown that the

stripe antiferromagnetism is stabilized by ferro-orbital order which breaks the in-plane lattice symmetry and induces a strong anisotropy between the magnetic exchange couplings.

Since the C_4 lattice symmetry is broken by the orbital order and the accompanying orthorhombic distortion, the electronic structure must reflect this spatial anisotropy with reduced symmetry.⁵³ Indeed, such an anisotropic electronic state has been confirmed recently in scanning-tunneling-microscopy (STM)⁵⁴ and in-plane resistivity measurements.^{55,56} Dramatic Fermi-surface reconstructions at the structural transition,⁵⁷ as well as enormous transport⁵⁸ and phonon⁵⁹ anomalies, have been interpreted as indirect evidence for orbital ordering. Hence, on this interpretation, it is the orbital ordering that underlies the electronic anisotropy, not an inherent anisotropy due entirely to the electrons, indicative of a true nematic state.

Consequently, an open problem with the pnictides is the role itinerancy and local physics play in mediating the apparently unfrustrated anisotropic magnetism. In this work, we start from the idea of the ‘local-itinerant dichotomy’^{20,60,61} of the iron pnictides and motivate an effective degenerate double-exchange (DDEX) model, very similar to the ones used to describe metallic manganites with orbital degeneracies.^{62–64} To be more precise, we assume a ferromagnetic Hund coupling between the itinerant bands of the doubly-degenerate d_{xz} and d_{yz} orbitals and the local moments, which are described by the aforementioned J_1 - J_2 Heisenberg model. In the context of the manganites it has been shown^{62–64} that such DDEX models exhibit phases with long-range stripe-antiferromagnetic order. Despite the antiferromagnetic couplings between local-moment spins, ferromagnetic spin chains are stabilized by emergent ferro-orbital order. In this phase, the itinerant electrons are directed predominantly along the chains which minimizes the kinetic energy and gives rise to a highly anisotropic electronic state. Moreover, the double exchange is expected to strongly suppress the effective coupling between local moments along the chains, and possibly to make it even ferromagnetic.⁶⁵

In this work, we analyze the effective DDEX model and indeed find that the orbitally ordered $(\pi, 0)$ antiferromagnet is stable over a realistic parameter range for the parent iron-pnictide materials. In particular, the seizable next-nearest neighbor superexchange J_2 further stabilizes this phase. Whereas these results are to a large extent not surprising given the similarities with the manganites, the magnetic excitation spectra so far have been calculated only for a ladder system.⁶⁶ For the manganites, the DDEX model is usually simplified^{62–64} by treating the core spins as classical and by taking the limit of large or infinite Hund’s coupling J_H which is not justified for the pnictides. Here, we instead focus on the regime of small and intermediate J_H and develop the tools to calculate the magnetic excitation spectra in the presence of both, super- and double-exchange to linear-spin-wave

order. The spectra are found to be in good agreement with the neutron scattering data.⁴⁶ In particular, in some parameter space the double exchange along the ferromagnetic chains can overcompensate the bare antiferromagnetic superexchange as suggested by the experiment.

This paper is organized as follows. In Sec. II, we construct the local-itinerant, DDEX model. Sec. III deals with the methods we use to calculate the magnetic excitation spectra. In Sec. IV, we summarize our results, including ferro-orbital ordering, the spin-wave dispersions, and the magnetic anisotropies. Finally Sec. V discusses several aspects of our theory and validates its applicability to the pnictides.

II. MODEL

In this Section, we proceed to motivate the DDEX model for the pnictides. This model accounts for the presence of local moments, as suggested by the neutron-scattering experiments, as well as itinerant electrons responsible for the bad-metal behavior of the parent compounds. Moreover, the orbital degeneracy in combination with Hund’s coupling between electronic and spin degrees of freedom gives rise to orbital-ordering physics beyond simple band-structure theory. The Hamiltonian consists of three parts,

$$\mathcal{H} = \mathcal{H}_{\text{loc}} + \mathcal{H}_{\text{it}} + \mathcal{H}_H, \quad (1)$$

where \mathcal{H}_{loc} describes the superexchange couplings between local moments, \mathcal{H}_{it} the itinerant electrons of the degenerate d_{xz} and d_{yz} orbitals, and \mathcal{H}_H the ferromagnetic Hund coupling between local moments and itinerant electrons. In order for this model to be valid, Hund’s coupling J_H should be small compared to the tetrahedral crystal-field splitting between the t_{2g} and e_g multiplets, but larger than the tetragonal splitting between the d_{xy} orbital and the degenerate d_{xz}, d_{yz} doublet.⁴⁰

The local moments with spin S are coupled by superexchanges J_1 and J_2 between nearest and next-nearest neighbors, respectively. The corresponding Heisenberg Hamiltonian reads

$$\mathcal{H}_{\text{loc}} = \frac{J_1}{S^2} \sum_{\langle i,j \rangle} \mathbf{S}_i \cdot \mathbf{S}_j + \frac{J_2}{S^2} \sum_{\langle\langle i,j \rangle\rangle} \mathbf{S}_i \cdot \mathbf{S}_j, \quad (2)$$

where, for convenience, the superexchanges are measured in units of S^2 . Likewise, Hund’s exchange J_H which couples the electron spins to the local moments will be measured in units of S . This convention will facilitate our large- S expansion later. The superexchanges are mediated by virtual hopping processes via the p -orbitals of the arsenic ions which have alternating positions above and below the iron plaquettes. Certainly, a quantitative comparison of the exchange couplings would require knowledge of the two different Fe-As-Fe bond angles and the precise shape of the orbitals. Assuming that the virtual

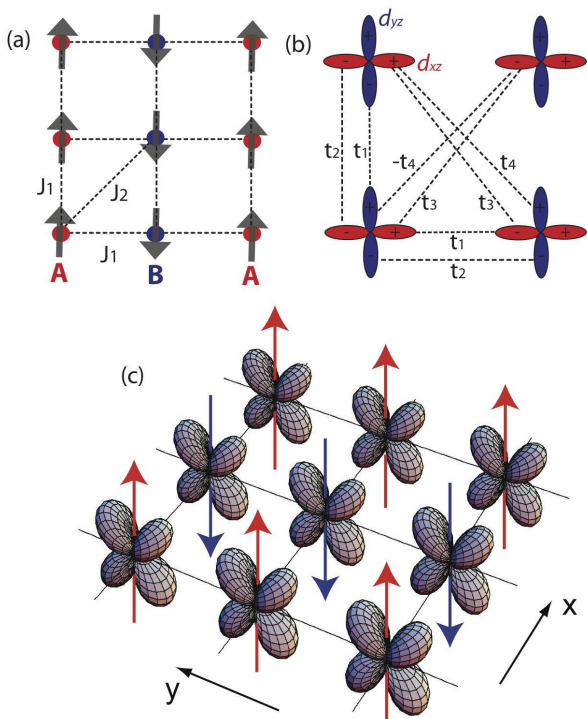


FIG. 1: (Color online) Illustration of the degenerate double-exchange model for the pnictides. (a) The local moments are coupled by nearest- and next-nearest-neighbor exchanges J_1 and J_2 , respectively, and interact via a ferromagnetic Hund coupling J_H with the itinerant electrons of the degenerate d_{xz} , d_{yz} orbitals. (b) Illustration of the hopping parameters in a two-band model of these orbitals (shown as projections in the plane). (c) Resulting ferro-orbital order which stabilizes $(\pi, 0)$ antiferromagnetism by directing the kinetic energy of the electrons along the ferromagnetic spin direction.

processes for the nearest-neighbor and diagonal bonds involve roughly the same energies, we estimate $J_1 \approx 2J_2$ since two exchange paths via different arsenic ions contribute to J_1 . Therefore, we expect the Heisenberg model (2) to be strongly frustrated and potentially in the quantum disordered regime.

The itinerant electrons of the degenerate d_{xz} and d_{yz} orbitals are described by a tight-binding Hamiltonian

$$\mathcal{H}_{\text{it}} = - \sum_{ij, \alpha\beta, \nu} t_{ij}^{\alpha\beta} c_{i\alpha\nu}^\dagger c_{j\beta\nu}, \quad (3)$$

where $c_{i\alpha\nu}^\dagger$ creates an electron with spin ν at site i on orbital α . The hopping integrals $t_{ij}^{\alpha\beta}$ are illustrated in Fig. 1(b) and defined in the same way as in Ref. 32. For simplicity, we neglect inter- and intra-orbital Coulomb repulsions⁶⁷ between the itinerant electrons. This is justified since on the level of the effective DDEX model, the local moments are formed as a consequence of strong correlations whereas the residual charge carriers should

be viewed as weakly interacting quasiparticles. We will assume t_1 to be the dominant hopping because a larger wave-function overlap is expected when the orbitals point towards one another. However, the precise shape of the orbitals is not determined by geometry but depends on quantum chemistry, for example, on the amount of hybridization between the Fe d - and As p -orbitals.²⁰ Here we simply denote the orbitals by d_{xz} and d_{yz} because of the spatial symmetry shared with the atomic Fe orbitals. Recently, it has been suggested⁵¹ that the hybridization leads to a strong deformation of the orbitals which make the π overlap, t_2 the dominant one. We point out that our results persist for the exchange of t_1 and t_2 , the only difference being that the orbital polarization will be inverted in order to maximize the overlap along the ferromagnetic spin direction.

We do not attempt to fit our hopping parameters to reproduce the electron and hole pockets as has been done in previous two-orbital models^{32,68} at the level of a tight-binding approximation. Such parameters are inherently arbitrary since the hopping amplitudes are not uniquely determined by a particular constant energy cut⁶⁸ and because Coulomb interactions and Hund's exchange are of the order of the electronic bandwidth.^{21–26} Moreover, the Fermi surfaces in the antiferromagnetically ordered phase have not been clearly established yet.

Finally the local moments and the itinerant electrons interact by a ferromagnetic Hund coupling,

$$\mathcal{H}_H = - \frac{J_H}{2S} \sum_{i, \alpha, \nu\nu'} \mathbf{S}_i \cdot c_{i\alpha\nu}^\dagger \boldsymbol{\sigma}_{\nu\nu'} c_{i\alpha\nu}, \quad (4)$$

where $\boldsymbol{\sigma}_{\nu\nu'} = (\sigma^x, \sigma^y, \sigma^z)_{\nu\nu'}$ with σ^α the standard Pauli matrices and $J_H > 0$. As mentioned before, Hund's exchange is measured in units of the local moment S . We note that similar models have been proposed in the context of the pnictides.^{60,61} However, the orbital degeneracy which is the pre-requisite for orbital-ordering physics and the resulting spatial anisotropies has not been included.

III. METHOD

In this Section, we outline the approximations and transformation we employ to analyze the complicated DDEX model for the pnictides. In similar models for the manganites, the problem is typically simplified by treating the local moments as classical spins and assuming an infinitely strong Hund exchange.^{62–64} In the pnictides, these approximations are not justified since the Hund coupling is of the order of the electronic bandwidth and since the local moments are small and presumably best described by the extreme quantum limit, $S = 1/2$. Moreover, our goal is the calculation of the magnetic excitation spectra which will require the inclusion of quantum fluctuations of the spins. Although the spins are small and the Heisenberg model \mathcal{H}_{loc} is strongly frustrated, it

is reasonable to treat the local moments on the level of linear spin-wave theory since the double exchange is expected to lead to a dramatic stabilization of the magnetic order. Moreover, it has been argued that the $1/S$ expansion is much better behaved for $(\pi, 0)$ order as compared to conventional (π, π) Néel antiferromagnetism.⁴²

Since Hund's coupling \mathcal{H}_H does not conserve the magnons describing the spin-wave excitation of the isolated local moments, we perform a canonical transformation in order to identify the true magnons of the coupled system. Readers not interested in the details of this calculation can skip immediately to the results, Sec. IV.

A. Operator rotations

Following the standard treatment of the antiferromagnetic Heisenberg model, we perform the spin rotation $S_i^x = \tilde{S}_i^x$, $S_i^y = \kappa_i \tilde{S}_i^y$, and $S_i^z = \kappa_i \tilde{S}_i^z$ where $\kappa_i = \exp(i\mathbf{Q} \cdot \mathbf{r}_i) = \pm 1$ for sublattices A and B, respectively [see Fig. 1(a)]. Representing the rotated spin operators \tilde{S}_i by Holstein-Primakoff (HP) bosons a_i, a_i^\dagger , to the leading order, $\tilde{S}_i^z = S - a_i^\dagger a_i$, $\tilde{S}_i^+ = \sqrt{2S} a_i$, and $\tilde{S}_i^- = a_i^\dagger \sqrt{2S}$ ($\tilde{S}_i^\pm = \tilde{S}_i^x \pm i\tilde{S}_i^y$), we immediately derive the following expression for \mathcal{H}_{loc} in the linear spin-wave approximation,

$$\mathcal{H}_{\text{loc}}^{\text{sw}} = \sum_q \left[A_0(q) \left(a_q^\dagger a_q + a_{-q} a_{-q}^\dagger \right) + B_0(q) \left(a_q^\dagger a_{-q}^\dagger + a_{-q} a_q \right) \right], \quad (5)$$

where $A_0(q) = (J_1 \cos q_y + 2J_2)/S$ and $B_0(q) = (J_1 \cos q_x + 2J_2 \cos q_x \cos q_y)/S$.

In order to leave Hund's coupling term \mathcal{H}_H invariant, we perform exactly the same rotation of the electron spins $s_{i\alpha} = \frac{1}{2} \sum_{\nu\nu'} c_{i\alpha\nu}^\dagger \boldsymbol{\sigma}_{\nu\nu'} c_{i\alpha\nu'}$. This is achieved by transforming the fermion operators as $c_{i\alpha\nu} = \tilde{c}_{i\alpha\nu}$ for sites i on sublattice A and $c_{i\alpha\nu} = \tilde{c}_{i\alpha\bar{\nu}}$ on sublattice B. In the latter expression, we have defined $\bar{\nu} = \downarrow$ for $\nu = \uparrow$ and vice versa. In terms of the HP boson creation and annihilation operators a_i, a_i^\dagger and rotated fermion operators $\tilde{c}_{i\alpha\nu}$, $\tilde{c}_{i\alpha\nu}^\dagger$ Hund's exchange can be written as

$$\mathcal{H}_H = \mathcal{H}_H^{(0)} + \mathcal{H}_H^{(1)} + \mathcal{H}_H^{(2)}, \quad (6)$$

$$\mathcal{H}_H^{(0)} = -\frac{J_H}{2} \sum_{k,\alpha,\nu} \nu \tilde{c}_{k\alpha\nu}^\dagger \tilde{c}_{k\alpha\nu}, \quad (7)$$

$$\mathcal{H}_H^{(1)} = -\frac{J_H}{\sqrt{2S}} \sum_{kq,\alpha} \left(a_q \tilde{c}_{k+q,\alpha\downarrow}^\dagger \tilde{c}_{k\alpha\uparrow} + \text{h.c.} \right), \quad (8)$$

$$\mathcal{H}_H^{(2)} = \frac{J_H}{2S} \sum_{k,qq',\alpha\nu} \nu a_q^\dagger a_{q'} \tilde{c}_{k-q,\alpha\nu}^\dagger \tilde{c}_{k-q',\alpha\nu}, \quad (9)$$

where $\nu = \pm 1$ for up and down spins, respectively. Note that $\mathcal{H}_H^{(0)}$ only involves the electronic operators and represents the zeroth-order corrections to the electron energies by the classical background stripe antiferromagnetism. $\mathcal{H}_H^{(1)}$ and $\mathcal{H}_H^{(2)}$ are the couplings between the

electrons and the HP bosons, linear and quadratic in the boson operators. In the following, we include the term $\mathcal{H}_H^{(0)}$ in the itinerant-electron Hamiltonian, yielding the effective free-electron Hamiltonian

$$\begin{aligned} \mathcal{H}_e &= \mathcal{H}_{\text{it}} + \mathcal{H}_H^{(0)} \\ &= \sum_{k,\alpha,\nu} \left[\left(\varepsilon_1^\alpha(k) - \nu \frac{J_H}{2} \right) \tilde{c}_{k\alpha\nu}^\dagger \tilde{c}_{k\alpha\nu} \right. \\ &\quad \left. + \varepsilon_2^\alpha(k) \tilde{c}_{k\alpha\nu}^\dagger \tilde{c}_{k\alpha\bar{\nu}} + \varepsilon_3(k) \tilde{c}_{k\alpha\nu}^\dagger \tilde{c}_{k\alpha\bar{\nu}} \right], \quad (10) \end{aligned}$$

where $\bar{\alpha} = yz$ for $\alpha = xz$ and vice versa. We have defined $\varepsilon_1^{xz}(k) = -2t_2 \cos k_y$, $\varepsilon_1^{yz}(k) = -2t_1 \cos k_y$, $\varepsilon_2^{xz}(k) = -2t_1 \cos k_x - 4t_3 \cos k_x \cos k_y$, $\varepsilon_2^{yz}(k) = -2t_2 \cos k_x - 4t_3 \cos k_x \cos k_y$, and $\varepsilon_3(k) = -t_4 \sin k_x \sin k_y$.

B. Canonical transformation

Apparently, the interaction term $\mathcal{H}_H^{(1)}$ is linear in the HP-boson operators, which shows that these bosons do not represent the Goldstone modes of the system, namely the transverse fluctuations of the total staggered magnetic moments, which consist of not only the local moments, but also the spins of the itinerant electrons. In order to correctly identify the true magnons and carry out the subsequent spin-wave calculations, we need to perform a canonical transformation of the original Hamiltonian $\mathcal{H} = \mathcal{H}_{\text{loc}}^{\text{sw}} + \mathcal{H}_e + \mathcal{H}_H^{(1)} + \mathcal{H}_H^{(2)}$,

$$\begin{aligned} \mathcal{H}' &= e^{\Delta} \mathcal{H} e^{-\Delta} \\ &= \mathcal{H} + [\Delta, \mathcal{H}] + \frac{1}{2} [\Delta, [\Delta, \mathcal{H}]] + \dots \quad (11) \end{aligned}$$

with Δ a suitable anti-Hermitian operator, $\Delta^\dagger = -\Delta$, such that in the transformed \mathcal{H}' , the terms linear in a_i 's are eliminated. Similar canonical transformations^{69,70} and equivalent perturbative methods⁷¹ have been used to explain ferromagnetism in double-exchange models with a single itinerant band. Up to the leading order, the transformation is determined by

$$[\Delta, \mathcal{H}_e] + \mathcal{H}_H^{(1)} = 0. \quad (12)$$

To find the Δ satisfying (12), we first diagonalize \mathcal{H}_e by a unitary transformation $\tilde{c}_{k\alpha\nu} = \sum_n U_{\alpha\nu}^n(k) d_{nk}$, yielding $\mathcal{H}_e = \sum_{n,k} E_n(k) d_{nk}^\dagger d_{nk}$. Here, n labels the four electronic bands arising after diagonalization from the two orbital and two spin degrees of freedom. In the new basis of d_{nk} , it is easy to verify that (12) is solved by

$$\begin{aligned} \Delta &= \frac{J_H}{\sqrt{2S}} \sum_{kq,mn,\alpha} \left(\frac{a_q d_{m,k+q}^\dagger d_{nk}}{E_n(k) - E_m(k+q)} \right. \\ &\quad \left. \times U_{\alpha\downarrow}^{m*}(k+q) U_{\alpha\uparrow}^n(k) - \text{h.c.} \right). \quad (13) \end{aligned}$$

After the canonical transformation (11), the Hamiltonian up to order $1/S$ reads $\mathcal{H}' = \mathcal{H}_e + \mathcal{H}_{\text{loc}}^{\text{sw}} + \mathcal{H}_{\text{H}}^{(2)} + \mathcal{H}'_2$, where $\mathcal{H}'_2 = [\Delta, \mathcal{H}_{\text{H}}^{(1)}] + \frac{1}{2}[\Delta[\Delta, \mathcal{H}_e]] = \frac{1}{2}[\Delta, \mathcal{H}_{\text{H}}^{(1)}]$. The commutators $[\Delta, \mathcal{H}_{\text{loc}}^{\text{sw}}]$ and $[\Delta, \mathcal{H}_{\text{K}}^{(2)}]$ are of higher orders in $1/S$ and the boson operators, and thus can be dropped in the linear spin-wave approximation. The contributions $\mathcal{H}_{\text{H}}^{(2)}$ and \mathcal{H}'_2 are bilinear in both, the bosonic and fermionic operators. After taking the expectation values of the electronic operators with respect to the diagonal electronic Hamiltonian \mathcal{H}_e , we obtain the final spin-wave Hamiltonian

$$\begin{aligned} \mathcal{H}^{\text{sw}} &= \mathcal{H}_{\text{loc}}^{\text{sw}} + \left\langle \mathcal{H}_{\text{H}}^{(2)} + \frac{1}{2}[\Delta, \mathcal{H}_{\text{H}}^{(1)}] \right\rangle_e \\ &= \sum_q \left[A(q) \left(a_q^\dagger a_q + a_{-q} a_{-q}^\dagger \right) \right. \\ &\quad \left. + B(q) \left(a_q^\dagger a_{-q}^\dagger + a_{-q} a_q \right) \right] \end{aligned} \quad (14)$$

with $A(q) = A_0(q) + A_1 + A_2(q)$ and $B(q) = B_0(q) + B_2(q)$. The constant ‘self-energy’ correction, A_1 arises from $H_{\text{K}}^{(2)}$ whereas $H'_2 = \frac{1}{2}[\Delta, \mathcal{H}_{\text{H}}^{(1)}]$ generates momentum-dependent corrections to both, the ‘self-energy’ and the ‘anomalous amplitude’, which are denoted as $A_2(q)$ and $B_2(q)$. These corrections are expressed as

$$A_1 = \frac{J_{\text{H}}}{2S} \sum_{k,n} f_n(k) \sum_{\alpha,\nu} \nu |U_{\alpha\nu}^n(k)|^2, \quad (15)$$

$$\begin{aligned} A_2(q) &= \frac{J_{\text{H}}^2}{2S} \sum_{k,mn} \frac{f_n(k) - f_m(k+q)}{E_n(k) - E_m(k+q)} \\ &\quad \times \left| \sum_{\alpha} U_{\alpha\downarrow}^{m*}(k+q) U_{\alpha\uparrow}^n(k) \right|^2, \end{aligned} \quad (16)$$

$$\begin{aligned} B_2(q) &= \frac{J_{\text{H}}^2}{2S} \sum_{k,mn} \frac{f_n(k) - f_m(k+q)}{E_n(k) - E_m(k+q)} \\ &\quad \times \sum_{\alpha\beta} U_{\alpha\downarrow}^{m*}(k+q) U_{\alpha\uparrow}^n(k) U_{\beta\downarrow}^{n*}(k) U_{\beta\uparrow}^m(k+q), \end{aligned} \quad (17)$$

where $f_n(k) = 1/(1 + e^{\beta(E_n(k) - \mu)})$ denotes the Fermi-distribution function with μ the chemical potential. The Hamiltonian (14) is diagonalized by a Bogoliubov transformation yielding the spin-wave dispersion

$$\omega(q) = \sqrt{A^2(q) - B^2(q)} \quad (18)$$

of the system in the presence of both, super- and double-exchange.

IV. RESULTS

A. Classical phase diagram

As a pre-requisite for the spin-wave expansion, we first have to identify the regime where $(\pi, 0)$ stripe antiferromagnetism is classically stable. When $J_{\text{H}} = 0$ or at

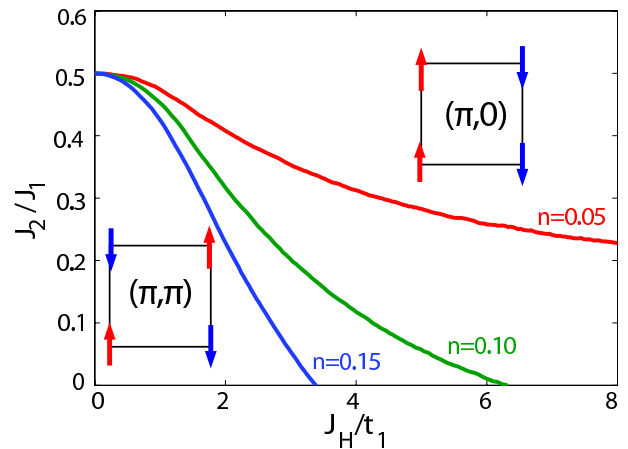


FIG. 2: (Color online) Classical phase diagrams of the degenerate double-exchange model as a function of J_{H}/t_1 and J_2/J_1 for different filling levels $n = 0.05$, $n = 0.10$, and $n = 0.15$. The tight-binding hopping parameters are $t_2 = -0.1t_1$, $t_3 = 0.2t_1$, and $t_4 = 0.05t_1$, the nearest-neighbor superexchange $J_1 = 0.04t_1$.

zero filling ($n = 0$), $(\pi, 0)$ order is stable for $J_2 > J_1/2$. In this regime, a finite Hund coupling further stabilizes $(\pi, 0)$ order since the itinerant electrons are more likely to occupy the d_{yz} orbitals which have a larger overlap along the ferromagnetic y -direction. Hence the double-exchange effectively weakens the spin coupling along the y direction and reduces the magnetic frustration. On the other hand, for $J_2 < J_1/2$ the (π, π) Néel antiferromagnet is the classical ground state for $J_{\text{H}} \rightarrow 0$. However, from the DDEX models for the manganites, it is known^{62–64} that even for $J_2 = 0$, a sufficiently strong Hund coupling will eventually stabilize $(\pi, 0)$ order.

For $J_2 < J_1/2$, the phase boundary between the two classical ground states is determined by the condition that the electronic kinetic-energy gain for the orbitally-polarized and stripe-ordered configuration equals the difference of the magnetic energies, $E_{(\pi,0)} - E_{(\pi,\pi)} = 2J_1 - 4J_2$. The electronic energies for a given electron filling n are easily calculated by diagonalizing the free-electron Hamiltonian \mathcal{H}_e (10) for the two different spin configurations. From now on, all the energies will be expressed in the unit of t_1 , the largest of the hopping amplitudes. The tight-binding parameters will be chosen to be $t_2 = -0.1t_1$, $t_3 = 0.2t_1$, and $t_4 = 0.05t_1$ throughout the paper. We further set $J_1 = 0.04t_1$ so that the exchange constants are of the order of 10 meV for a bandwidth of 1 eV, in agreement with both numerical³⁹ and experimental⁴⁶ observations.

The resulting phase diagrams for electron fillings $n = 0.05$, $n = 0.1$, and $n = 0.15$ are shown in Fig. 2. As predicted, a sufficiently large J_{H} can stabilize $(\pi, 0)$ stripe order even when Néel order is favored by $J_2 < J_1/2$. Moreover, the $(\pi, 0)$ phase is enhanced for larger filling n because the kinetic energy gain increases with the number of itinerant electrons. Although similar results have

been obtained in the context of the manganites,^{62–64} we point out that there are crucial differences. Whereas in the manganites J_2 is negligible and $(\pi, 0)$ antiferromagnetism obtains because of the enormously large Hund coupling, in the pnictides, J_H is much smaller and of the order of the electronic bandwidth.^{21–26} Therefore, the large J_2 , which has been predicted early on²⁷ based on the geometry of the ion-arsenic layers, is essential for stripe antiferromagnetism in the pnictides.

In the following calculations we will mostly focus on the regime $J_2 > J_1/2$, where $(\pi, 0)$ order remains classically stable for $J_H \rightarrow 0$. In the calculation, our primary interest is in how the spin-wave spectrum is renormalized as we gradually turn on J_H . In principle, when $J_2 < J_1/2$, the linear spin-wave calculations can still be carried out for a J_H that is large enough to classically stabilize the stripe order.

B. Orbital and spin polarization

We proceed with a more careful inspection of the electronic Hamiltonian \mathcal{H}_e (10) which includes Hund's coupling to the local moments on a classical level given by $\mathcal{H}_H^{(0)}$. Here we focus on the regime where the classical magnetic ground state $\kappa_i = \exp(i\mathbf{Q} \cdot \mathbf{r}_i) = \pm 1$ is the stripe antiferromagnet, $\mathbf{Q} = (\pi, 0)$. Certainly, this is always the case for $J_2 > J_1/2$. From the diagonalization of \mathcal{H}_e (10) with the same set of hopping parameters used previously, we obtain the dispersions of the electronic bands $E_n(k)$ shown in Fig. 3(a) and (b) for $J_H = 0.1t_1$ and $J_H = 1.0t_1$, respectively. Since the diagonal hopping amplitude t_4 between different orbitals is non-zero, the bands are always momentum-dependent superpositions of the two orbitals d_{yz} and d_{xz} as indicated by the color coding. For small J_H [Fig. 3(a)], the orbital hybridization is found to be strong for some momenta, for example, along the $(0, 0)$ - (π, π) direction. However, in the relevant regime where Hund's coupling is of the order of the electronic bandwidth, e.g. $J_H = 1.0t_1$ [Fig. 3(b)], the gaps between the bands are pronounced and the orbital polarization of each band remains almost perfect for all momenta. Therefore, from now on, we will denote these bands as ' d_{xz} ' and ' d_{yz} ' for simplicity.

We further calculate the total orbital polarization $n_o = \sum_\nu (\rho_{yz,\nu} - \rho_{xz,\nu})$ and spin polarization $n_s = \sum_\alpha (\rho_{\alpha,\uparrow} - \rho_{\alpha,\downarrow})$. Here, $\rho_{\alpha\nu} = \langle \tilde{c}_{i\alpha\nu}^\dagger \tilde{c}_{i\alpha\nu} \rangle$ is defined as the density of electrons in orbital $\alpha = xz, yz$ with spin $\nu = \uparrow, \downarrow$. Obviously, these densities sum up to the total filling of the bands, $n = \sum_{\alpha\nu} \rho_{\alpha\nu}$. Note that since the densities are defined in the sub-lattice rotated basis, $\nu = \uparrow$ corresponds to an electron spin aligned with the local moment spin.

In Fig. 3(c), the orbital polarization n_o is shown as a function of the total filling n for different values of J_H . For small n the electrons populate only the lowest band with almost perfect d_{yz} character and therefore $n_o \simeq n$. Indeed, the slope is very close to one indicating that the

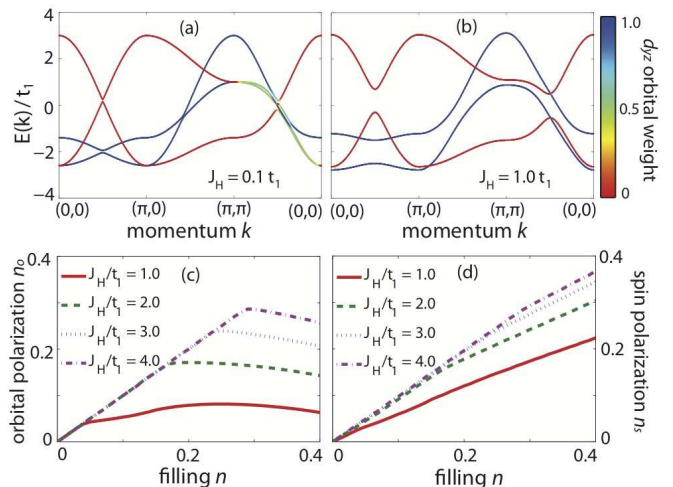


FIG. 3: (Color online) (a, b) The dispersions of the itinerant-electron bands for $J_H = 0.1t_1$ (a) and $J_H = 1.0t_1$ (b), along the path $(0, 0)$ - $(\pi, 0)$ - (π, π) - $(0, 0)$ in the Brillouin zone containing one Fe atom per unit cell. The tight-binding parameters are chosen to be $t_2 = -0.1t_1$, $t_3 = 0.2t_1$, and $t_4 = 0.05t_1$ throughout the paper. The bands are colored according to the weight of the d_{yz} orbital. (c, d) Total orbital polarization n_o (c) and spin polarization n_s (d) as a function of the filling n for various Hund's couplings J_H .

admixture of the d_{xz} orbital to the lowest band is negligible and that the orbital polarization can be considered to be perfect. The emergent ferro-orbital order, illustrated in Fig. 1, is a consequence of the ferromagnetic Hund's coupling which wants to align the electron spin with the local moments and therefore suppresses the electron motion along the antiferromagnetic spin direction. Since $t_1 > |t_2|$ the electrons populate the d_{yz} orbitals which have a larger overlap along the ferromagnetic y direction. Increasing the filling n , the Fermi energy will eventually reach the bottom of the next band with mainly d_{xz} character. Above this particular filling \bar{n} , the orbital polarization is no longer perfect and even starts to decrease with n for larger values of J_H . In general, a larger J_H increases the energy difference between the two bands, and thus increases the filling \bar{n} up to which the orbital polarization is perfect.

Since Hund's coupling tends to align the spins of the itinerant electrons with the local moments, also the spin polarization n_s increases with the electron filling n and is bigger for larger J_H as shown in Fig. 3(d). However, for small n , the slopes are slightly smaller than one, signaling an incomplete spin polarization. This is a consequence of the small but finite spin off-diagonal elements in \mathcal{H}_e (10) which do not only depend on the smallest hopping amplitude t_4 , as the orbital hybridization terms, but also on t_2 and t_3 . For $n > \bar{n}$, the slope of the spin-polarization curves is reduced indicating that the spin polarization of the d_{yz} orbitals is larger than that of the d_{xz} orbitals.

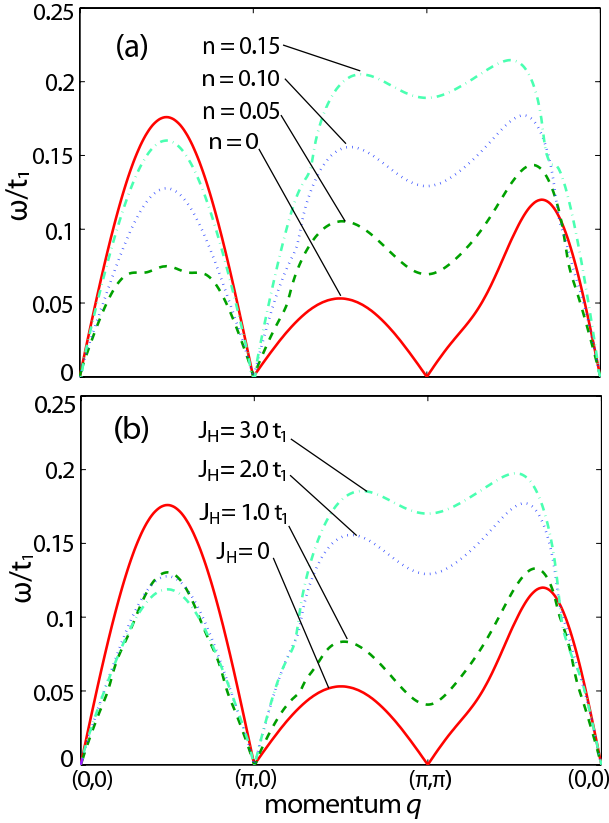


FIG. 4: (Color online) Spin-wave dispersion $\omega(q)$ in the presence of both super- and double-exchange along the path $(0, 0)$ - $(\pi, 0)$ - (π, π) - $(0, 0)$ for (a) different filling levels n , $J_H = 2.0t_1$, and (b) different Hund's couplings J_H , $n = 0.1$. In both cases, $J_1 = 0.04t_1$, $J_2 = 0.6J_1$, and $S = 1/2$.

C. Spin-wave spectrum

Now we set out to calculate the spin-wave spectrum by considering the corrections from the itinerant bands to the J_1 - J_2 Heisenberg model for the local moments. The hopping amplitudes are set to the values used before. The spin length S of the local moment is $1/2$, which reflects the relatively small moment measured by the experiment¹⁰ and is consistent with a local multiplet structure with an orbital degeneracy.⁴⁰ Finally, the Heisenberg model is strongly frustrated with $J_1 = 0.04t_1$ and $J_2 = 0.6J_1$.

We first calculate the spin-wave spectra for different filling levels n with $J_H = 2.0t_1$, shown by Fig. 4(a). In this case, the complete orbital polarization is found up to $\bar{n} = 0.16$ [see Fig. 3(c)]. When $n = 0$, corresponding to an empty itinerant band, our model reduces to an isotropic J_1 - J_2 Heisenberg model, where the linear spin-wave energies are zero at both, $(\pi, 0)$ and (π, π) . At finite electron densities $n < \bar{n}$, we observe that the spin-wave energy at (π, π) is pushed to higher values as n increases. This indicates a stabilization of the stripe antiferromagnetism over the competing Néel order. We also note a significant mode softening along the $(0, 0)$ - $(\pi, 0)$ direction at

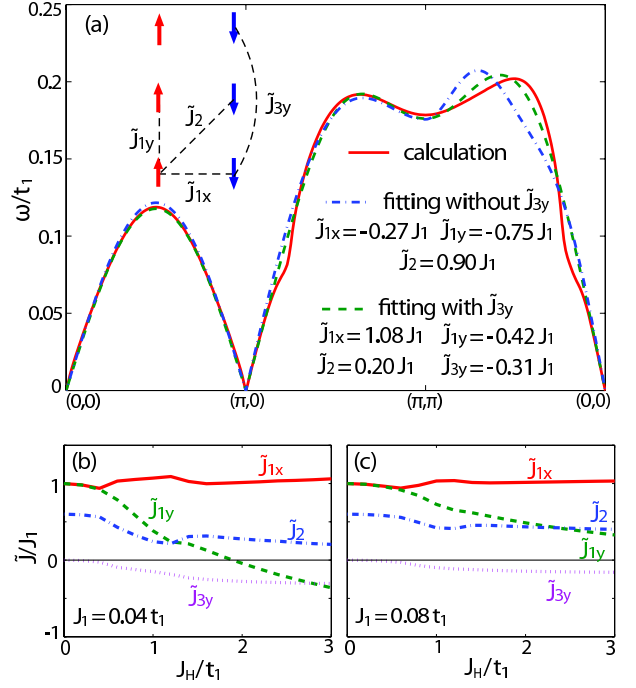


FIG. 5: (Color online) (a) Best fits of the spin-wave spectrum of the DDEX for $n = 0.1$ and $J_H = 3.0t_1$ obtained from a spin-only model with effective couplings illustrated as inset. (b, c) Effective exchange constants as functions of Hund's coupling J_H for bare exchange constants $J_1 = 0.04t_1$ (b), $J_1 = 0.08t_1$ (c), and $J_2/J_1 = 0.6$.

low fillings due to the other finite hopping amplitudes t_2 , t_3 , and t_4 .

For $n > \bar{n}$, not shown in the graph, the spin-wave energy at (π, π) decreases with n . This behavior results from the reduction of the orbital polarization [see Fig. 3(c)] and hence of the anisotropy, once the itinerant electrons populate the next band with mainly d_{xz} character. As the filling level continues to rise, the spin-wave spectrum becomes unstable suggesting that the system may evolve to a different ground state.

Fig. 4(b) shows the spin-wave spectra for different values of the Hund coupling J_H and a filling level of $n = 0.1$. According to Fig. 3(c), we have complete orbital polarization for all the J_H 's used in Fig. 4(b), except for $J_H = 1.0t_1$. As expected, a larger J_H produces stronger corrections to the spin-wave dispersion, especially around (π, π) where the spin-wave energy almost reaches a maximum. In contrast, the dispersion along $(0, 0)$ to $(\pi, 0)$ is almost unaffected after J_H reaches a certain value on the order of the electronic bandwidth.

D. Magnetic anisotropy

In Section IV C we saw that the double exchange leads to a dramatic change of the magnetic excitation spectra. In particular, the spin-wave modes at the Néel antiferro-

magnetic wave vector (π, π) are almost pushed to a maximum consistent with the neutron-scattering data.⁴⁶ Since orbital ordering leads to a dramatic anisotropy in the electronic structure, the ferromagnetic double-exchange contribution is expected to be much larger along the y -direction along where the ferromagnetic spin chains are formed. To quantify the induced magnetic anisotropy, in this Section, we fit the spin-wave dispersions calculated in the presence of both, super- and double-exchange to an effective, anisotropic Heisenberg model.

To be more specific, in the effective spin-only model, nearest-neighbors are coupled by exchanges \tilde{J}_{1x} and \tilde{J}_{1y} along the x and y directions, respectively, and next-nearest neighbors by \tilde{J}_2 [see inset of Fig. 5(a)]. Please note that different symbols are used here to distinguish from the couplings in the original Heisenberg model \mathcal{H}_{loc} (2). Furthermore, we introduce an additional ferromagnetic exchange $\tilde{J}_{3y} < 0$ between the third-nearest neighbors along the ferromagnetic chains. The utility of retaining longer-ranged ferromagnetic couplings has been demonstrated in the ferromagnetic double-exchange model, where simple nearest-neighbor exchange is unable to reproduce the calculated dispersions from either canonical transformations^{69,70} or diagrammatic perturbation theory.⁷¹ Also for manganites with so called CE-type charge-spin-orbital order, longer-ranged ferromagnetic couplings along the ferromagnetic zig-zag chains are crucial in order to obtain a good fit of the magnetic excitation spectra.⁶⁵

In the relevant regime $\tilde{J}_{1x} \geq \tilde{J}_{1y}$, $\tilde{J}_{1y} < 2\tilde{J}_2$, $\tilde{J}_{3y} < 0$, where $(\pi, 0)$ stripe antiferromagnetism is stable, the linear-spin wave dispersion $\tilde{\omega}(q)$ is determined by $\tilde{\omega}^2(q) = \tilde{A}^2(q) - \tilde{B}^2(q)$ with $\tilde{A}(q) = \tilde{J}_{1x} - \tilde{J}_{1y}(1 - \cos q_y) + 2\tilde{J}_2 - \tilde{J}_{3y}(1 - \cos 2q_y)$ and $\tilde{B}(q) = \tilde{J}_{1x} \cos q_x + 2\tilde{J}_2 \cos q_x \cos q_y$.

In Fig. 5(a), the fitted spin-wave dispersions to the spectrum calculated from the DDEX model with $n = 0.1$ and $J_H = 3.0t_1$ are shown. Indeed, the inclusion of the longer-ranged ferromagnetic coupling \tilde{J}_{3y} leads to a significant improvement of the fit. Moreover, setting $\tilde{J}_{3y} = 0$ gives an unrealistically large correction to the nearest-neighbor exchange along the x -direction ($\tilde{J}_{1x} = -0.27J_1$), which has to be compensated by a fairly substantial increase in the diagonal exchange, $\tilde{J}_2 = 0.90J_1$. This result is certainly unphysical since from the classical double-exchange argument, we expect $\tilde{J}_{1x} \simeq J_1$ and $\tilde{J}_2 < J_2$. In contrast, by including \tilde{J}_{3y} , we obtain more physical fitting results. Consequently, in the following, all of the fittings will be performed with $\tilde{J}_{3y} \neq 0$.

The resulting effective exchange constants as a function of Hund's coupling J_H are shown in Fig. 5(b) and (c) for $J_1 = 0.04t_1$ and $J_1 = 0.08t_1$, respectively. Note that for $J_1 = 0.04t_1$, the spectra of the DDEX model are shown in Fig. 4(b). In both cases we use $n = 0.1$, $J_2/J_1 = 0.6$, and the same tight-binding parameters as before. Obviously, for $J_H = 0$ the effective exchange constants have to be identical with the bare ones, $\tilde{J}_{1x} = \tilde{J}_{1y} = J_1$, $\tilde{J}_2 = J_2$, and $\tilde{J}_3 = 0$. Increasing Hund's coupling does

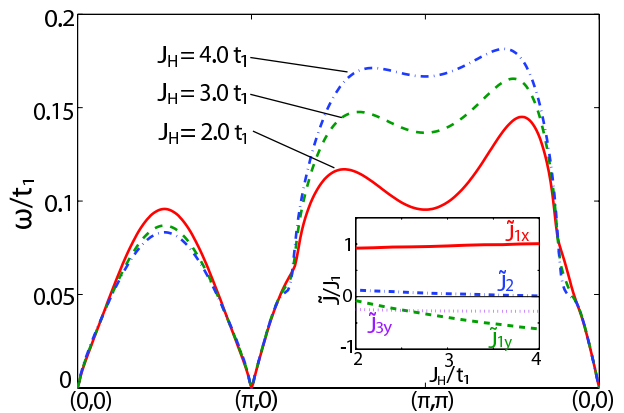


FIG. 6: (Color online) Spin-wave dispersion $\omega(q)$ in the presence of both, super- and double-exchange along the path $(0,0)$ - $(\pi,0)$ - (π,π) - $(0,0)$ for different Hund's couplings J_H . Parameters are the same as in Fig. 4(b), except for $J_2/J_1 = 0.4$. In this regime, $(\pi,0)$ order is classically stable for $J_H \gtrsim 1.6t_1$. (Inset: the fitted, effective exchange constants \tilde{J}_{1x} , \tilde{J}_{1y} , \tilde{J}_2 , and \tilde{J}_{3y} as functions of J_H .)

not change \tilde{J}_{1x} , whereas the other exchanges decrease due to the different ferromagnetic double-exchange contributions. Since t_1 is the largest hopping amplitude and most electrons populate the d_{yx} orbitals, the fastest decrease is observed for the coupling \tilde{J}_{1y} along the ferromagnetic chains. We also note that the non-monotonic behavior for small J_H is not unphysical, but due to the fact that for $n = 0.1$, complete orbital polarization is not achieved until $J_H \gtrsim 1.5t_1$.

Interestingly, in the case $J_1 = 0.04t_1$ [see Fig. 5(b)], the coupling \tilde{J}_{1y} along the ferromagnetic direction becomes negative for $J_H \gtrsim 2.0t_1$, which completely removes the frustration in the effective spin-only model. Such an effective negative exchange coupling along the ferromagnetic spin direction has been used phenomenologically to rationalize the spectra measured by inelastic neutron scattering.⁴⁶ Remarkably, around $J_H \approx 2.0t_1$, the ratios of the three exchange constants \tilde{J}_{1x} , \tilde{J}_{1y} , and \tilde{J}_2 , agree extremely well with the experimental estimates.⁴⁶ As shown in Fig. 5(c), for $J_1 = 0.08t_1$, the relative corrections to the exchange couplings are too small to make \tilde{J}_{1y} ferromagnetic for realistic values of J_H . In order to achieve the experimentally observed negative \tilde{J}_{1y} within reasonable parameter space, we require $J_1 \lesssim 0.05t_1$. In fact, inelastic neutron scattering⁴⁶ suggests that the exchange constants are of the order of 10 meV, which in our theory leads to an electronic bandwidth and Hund's coupling J_H both of the order of 1 eV, in agreement with other experimental estimates.²⁶

Though the parameter regime $J_2/J_1 < 1/2$ is most likely not relevant to the pnictides, we consider it nonetheless for completeness. In this regime, the Hund coupling has to exceed a critical value in order to stabilize $(\pi, 0)$ stripe antiferromagnetism. As an example, we assume $J_2 = 0.4J_1$ and $n = 0.1$, in which case $(\pi, 0)$ order

is classically stable for $J_H \gtrsim 1.6t_1$ [see Fig. 2]. The resulting spin-wave spectra are shown in Fig. 6 for different values of J_H . The effective exchange couplings obtained from fitting to the spin-only model are shown in the inset. Although the behavior is qualitatively similar to the case $J_2/J_1 = 0.6$, the agreement with the experimental data is not as good. Moreover, in order to push the dispersion at (π, π) close to a maximum, we need a much bigger J_H which can not be justified for the pnictides.

V. DISCUSSION AND CONCLUSION

In summary, we have studied a DDEX model for the iron pnictides which explains the dramatic magnetic^{45,46} and electronic^{54,56} anisotropies in these materials. The model consists of local moments which are coupled by antiferromagnetic superexchanges J_1 and J_2 between nearest- and next-nearest-neighbor spins, respectively, and of itinerant electrons in the bands of the degenerate d_{xz} and d_{yz} orbitals. The electrons are coupled to the local moments by a ferromagnetic Hund exchange, J_H . The system spontaneously develops ferro-orbital order because of the kinetic energy gained by directing the itinerant electrons along ferromagnetic spin chains which are stabilized by the double-exchange mechanism.

Although similar results have been obtained previously in the context of the manganites,⁶²⁻⁶⁴ we point out that there is a crucial difference between the two classes of materials. Whereas in the pnictides, the local moments are inherently quantum ($S = 1/2$) and J_H is at most of the order of the electronic bandwidth, the DDEX models for the manganites can be greatly simplified by assuming an infinitely large J_H and by treating the core spins as classical. Because of these approximations, the spin-wave excitations of the ferro-orbitally ordered stripe antiferromagnet have not been addressed in the manganite literature.

In this work, we have explicitly taken the quantum nature of the local moments into account and calculated the magnetic excitation spectra in the presence of both, super- and double-exchange. Over a realistic parameter range, the calculated spin-wave dispersions are found to be in good agreement with the neutron-scattering data.^{45,46} In particular, we find that the dispersion is pushed almost to a local maximum at the competing Néel ordering wave vector as seen in the experiment.⁴⁶ By fitting to an effective spin-only model, we find that the coupling along the ferromagnetic direction becomes negative, which demonstrates that in the pnictides, the double-exchange along the ferromagnetic spin-direction can overcompensate the superexchange between the local moments. In this regime, $(\pi, 0)$ antiferromagnetism is unfrustrated.

It is feasible that the parent, undoped materials self-tune the size of the local moments and the carrier density to the point where the $(\pi, 0)$ antiferromagnetism is most stable. In our theory, this is the case for the optimal filling level $n = \bar{n}$ where the orbital polarization reaches a maximum. In fact, the starting Heisenberg model \mathcal{H}_{loc} (2) is likely to be in the regime of strong frustration, $0.4 < J_2/J_1 < 0.6$, where quantum fluctuations destroy long range magnetic order. Only through the interaction with the itinerant electrons does stripe antiferromagnetism emerge. Electron- or hole-doping the system at $n = \bar{n}$ diminishes the orbital order and thus increases the magnetic frustration, lowering the transition temperature to a spin-ordered state.

We conclude by stressing that the degenerate double-exchange model motivated and studied in this work qualitatively explains many properties of the undoped and slightly doped iron pnictides. The emergent ferro-orbital order breaks the in-plane lattice symmetry, thereby driving the orthorhombic lattice distortion. Further, orbital order induces a strong electronic anisotropy which explains why the structural transition is accompanied by dramatic Fermi-surface reconstructions⁵⁷ and transport anomalies.⁵⁸ Moreover, recent STM experiments⁵⁴ and in-plane resistivity measurements^{55,56} have unambiguously demonstrated the spatial anisotropy of the electronic state at temperatures below the structural transition temperature. Finally, orbital ordering produces strong magnetic anisotropy, essential for explaining the experimentally observed magnetic excitation spectra.^{45,46}

During the review of this work, several mean-field calculations⁷²⁻⁷⁴ based on five-orbital Hubbard models have shown that the total occupations of the d_{xz} and d_{yz} orbitals are close to each other, but that there is a significant difference in the density of states for the two orbitals at the chemical potential. The ferro-orbital order in our theory does not contradict these results. In fact, by viewing the itinerant electrons as residual quasiparticles on top of local moments formed because of strong correlations, our model is an effective low-energy theory that successfully describes the strongly anisotropic electron state around the Fermi surface of the iron pnictides.

Acknowledgments

This work is partially funded by NSF under Grant No. DMR-0940992. The authors acknowledge support from the Center for Emergent Superconductivity, an Energy Frontier Research Center funded by the U.S. Department of Energy, Office of Science, Office of Basic Energy Sciences under Award Number DE-AC0298CH1088.

¹ Y. Kamihara, T. Watanabe, M. Hirano, and H. Hosono, *J. Am. Chem. Soc.* **130**, 3296 (2008).

² X. H. Chen, T. Wu, G. Wu, R. H. Liu, H. Chen, and D. F.

- Fang, *Nature (London)* **453**, 761 (2008).
- ³ G. F. Chen, Z. Li, D. Wu, G. Li, W. Z. Hu, J. Dong, P. Zheng, J. L. Luo, and N. L. Wang, *Phys. Rev. Lett.* **100**, 247002 (2008).
 - ⁴ Z. A. Ren, G. C. Che, X. L. Dong, J. Yang, W. Lu, W. Yi, X. L. Shen, Z. C. Li, L. L. Sun, F. Zhou, et al., *Europhys. Lett.* **83**, 17002 (2008).
 - ⁵ H. H. Wen, G. Mu, L. Fang, H. Yang, and X. Y. Zhu, *Europhys. Lett.* **82**, 17009 (2008).
 - ⁶ M. Rotter, M. Tegel, and D. Johrendt, *Phys. Rev. Lett.* **101**, 107006 (2008).
 - ⁷ S. A. Kivelson and H. Yao, *Nature Materials* **7**, 927 (2008).
 - ⁸ J. Zaanen, *Nature* **457**, 546 (2009).
 - ⁹ S. Tesanovic, *Physics* **2**, 60 (2009).
 - ¹⁰ C. de la Cruz, Q. Huang, J. W. Lynn, W. R. J. Li, J. L. Zarestky, H. A. Mook, G. F. Chen, J. L. Luo, N. L. Wang, and P. Dai, *Nature (London)* **453**, 899 (2008).
 - ¹¹ J. Zhao, Q. Huang, C. de la Cruz, S. Li, J. W. Lynn, Y. Chen, M. A. Green, G. F. Chen, G. Li, Y. Li, et al., *Nature Materials* **7**, 953 (2008).
 - ¹² J. Zhao, Q. Huang, C. de la Cruz, J. W. Lynn, M. D. Lumsden, Z. A. Ren, J. Yang, X. Shen, X. Dong, Z. Zhao, et al., *Phys. Rev. B* **78**, 132504 (2008).
 - ¹³ S. A. J. Kimber, D. N. Argyriou, F. Yokaichiya, K. Habicht, S. Gerischer, T. Hansen, T. Chatterji, R. Klingeler, C. Hess, G. Behr, et al., *Phys. Rev. B* **78**, 140503(R) (2008).
 - ¹⁴ A. I. Goldman, D. N. Argyriou, B. Ouladdiaf, T. Chatterji, A. Kreyssig, S. Nandi, N. Ni, S. L. Bud'ko, P. C. Canfield, and R. J. McQueeney, *Phys. Rev. B* **78**, 100506(R) (2008).
 - ¹⁵ J. Zhao, W. Ratcliff, J. W. Lynn, G. F. Chen, J. L. Luo, N. L. Wang, J. Hu, and P. Dai, *Phys. Rev. B* **78**, 140504(R) (2008).
 - ¹⁶ Q. Huang, Y. Qiu, W. Bao, M. A. Green, J. W. Lynn, Y. C. Gasparovic, T. Wu, G. Wu, and X. H. Chen, *Phys. Rev. Lett.* **101**, 257003 (2008).
 - ¹⁷ S. D. Wilson, Z. Yamani, C. R. Rotundu, B. Freelon, E. Bourret-Courchesne, and R. J. Birgeneau, *Phys. Rev. B* **79**, 184519 (2009).
 - ¹⁸ Y. Chen, J. W. Lynn, J. Li, G. Li, G. F. Chen, J. L. Luo, N. L. Wang, P. Dai, C. dela Cruz, and H. A. Mook, *Phys. Rev. B* **78**, 064515 (2008).
 - ¹⁹ J. Dong, H. J. Zhang, G. Xu, Z. Li, G. Li, W. Z. Hu, D. Wu, G. F. Chen, X. Dai, J. L. Luo, et al., *Europhys. Lett.* **83**, 27006 (2008).
 - ²⁰ J. Wu, P. Phillips, and A. H. C. Neto, *Phys. Rev. Lett.* **101**, 126401 (2008).
 - ²¹ K. Haule, J. H. Shim, and G. Kotliar, *Phys. Rev. Lett.* **100**, 226402 (2008).
 - ²² L. Craco, M. S. Laad, S. Leoni, and H. Rosner, *Physical Review B* **78**, 134511 (2008).
 - ²³ K. Nakamura, R. Arita, and M. Imada, *J. Phys. Soc. Japan* **77**, 093711 (2008).
 - ²⁴ V. Vildosola, L. Pourovskii, R. Arita, S. Biermann, and A. Georges, *Phys. Rev. B* **78**, 064518 (2008).
 - ²⁵ V. I. Anisimov, D. M. Korotin, S. V. Streltsov, A. V. Kozhevnikov, J. Kunes, A. O. Shorikov, and M. A. Korotin, *JETP Lett.* **88**, 729 (2008).
 - ²⁶ W. L. Yang, A. P. Sorini, C.-C. Chen, B. Moritz, W.-S. Lee, F. Vernay, P. Olalde-Velasco, J. D. Denlinger, B. Delley, J.-H. Chu, et al., *Phys. Rev. B* **80**, 014508 (2009).
 - ²⁷ Q. Si and E. Abrahams, *Phys. Rev. Lett.* **101**, 076401 (2008).
 - ²⁸ C. Fang, H. Yao, W.-F. Tsai, J. P. Hu, and S. A. Kivelson, *Phys. Rev. B* **77**, 224509 (2008).
 - ²⁹ C. Xu, M. Mueller, and S. Sachdev, *Phys. Rev. B* **78**, 020501(R) (2008).
 - ³⁰ I. I. Mazin, D. J. Singh, M. D. Johannes, and M. H. Du, *Phys. Rev. Lett.* **101**, 057003 (2008).
 - ³¹ K. Kuroki, S. Onari, R. Arita, H. Usui, Y. Tanaka, H. Kontani, and H. Aoki, *Phys. Rev. Lett.* **101**, 087004 (2008).
 - ³² S. Raghu, X.-L. Qi, C.-X. Liu, D. J. Scalapino, and S.-C. Zhang, *Phys. Rev. B* **77**, 220503(R) (2008).
 - ³³ A. V. Chubukov, D. V. Efremov, and I. Eremin, *Phys. Rev. B* **78**, 134512 (2008).
 - ³⁴ V. Cvetkovic and Z. Tesanovic, *Europhys. Lett.* **85**, 37002 (2009).
 - ³⁵ F. Wang, H. Zhai, Y. Ran, A. Vishwanath, and D.-H. Lee, *Phys. Rev. Lett.* **102**, 047005 (2009).
 - ³⁶ P. M. R. Brydon and C. Timm, *Phys. Rev. B* **80**, 174401 (2009).
 - ³⁷ J. Knolle, I. Eremin, A. V. Chubukov, and R. Moessner, *Phys. Rev. B* **81**, 140506 (2010).
 - ³⁸ Y.-Z. Zhang, I. Opahle, H. O. Jeschke, and R. Valentini, *Phys. Rev. B* **81**, 094505 (2010).
 - ³⁹ T. Yildirim, *Phys. Rev. Lett.* **101**, 057010 (2008).
 - ⁴⁰ F. Krüger, S. Kumar, J. Zaanen, and J. van den Brink, *Phys. Rev. B* **79**, 054504 (2009).
 - ⁴¹ H. C. Jiang, F. Krüger, J. E. Moore, D. N. Sheng, J. Zaanen, and Z. Y. Weng, *Phys. Rev. B* **79**, 174409 (2009).
 - ⁴² G. S. Uhrig, M. Holt, J. Oitmaa, O. P. Sushkov, and R. R. P. Singh, *Phys. Rev. B* **79**, 092416 (2009).
 - ⁴³ R. Applegate, J. Oitmaa, and R. R. P. Singh, *Phys. Rev. B* **81**, 024505 (2010).
 - ⁴⁴ B. Schmidt, M. Siahatgar, and P. Thalmeier, *Phys. Rev. B* **81**, 165101 (2010).
 - ⁴⁵ J. Zhao, D.-X. Yao, S. Li, T. Hong, Y. Chen, S. Chang, W. R. II, J. W. Lynn, H. A. Mook, G. F. Chen, et al., *Phys. Rev. Lett.* **101**, 167203 (2008).
 - ⁴⁶ J. Zhao, D. T. Adroja, D.-X. Yao, R. Bewley, S. Li, X. F. Wang, G. Wu, X. H. Chen, J. Hu, and P. Dai, *Nature Physics* **5**, 555 (2009).
 - ⁴⁷ P. Chandra and B. Doucot, *Phys. Rev. B* **38**, 9335 (1988).
 - ⁴⁸ C. L. Henley, *Phys. Rev. Lett.* **62**, 2056 (1989).
 - ⁴⁹ P. Chandra, P. Coleman, and A. I. Larkin, *Phys. Rev. Lett.* **64**, 88 (1990).
 - ⁵⁰ W. Lv, J. Wu, and P. Phillips, *Phys. Rev. B* **80**, 224506 (2009).
 - ⁵¹ C.-C. Lee, W.-G. Yin, and W. Ku, *Phys. Rev. Lett.* **103**, 267001 (2009).
 - ⁵² C.-C. Chen, B. Moritz, J. van den Brink, T. P. Devereaux, and R. R. P. Singh, *Phys. Rev. B* **80**, 180418 (2009).
 - ⁵³ W.-C. Lee and C. Wu, *Phys. Rev. Lett.* **103**, 176101 (2009).
 - ⁵⁴ T.-M. Chuang, M. P. Allan, J. Lee, Y. Xie, N. Ni, S. L. Budko, G. S. Boebinger, P. C. Canfield, and J. C. Davis, *Science* **327**, 181 (2010).
 - ⁵⁵ M. A. Tanatar, E. C. Blomberg, A. Kreyssig, M. G. Kim, N. Ni, A. Thaler, S. L. Budko, P. C. Canfield, A. I. Goldman, I. I. Mazin, et al., *Phys. Rev. B* **81**, 184508 (2010).
 - ⁵⁶ J.-H. Chu, J. G. Analytis, K. D. Greve, P. L. McMahon, Z. Islam, Y. Yamamoto, and I. R. Fisher (2010), arXiv:1002.3364.
 - ⁵⁷ T. Shimojima, K. Ishizaka, Y. Ishida, N. Katayama, K. Ohgushi, T. Kiss, M. Okawa, T. Togashi, X.-Y. Wang, C.-T. Chen, et al., *Phys. Rev. Lett.* **104**, 057002 (2010).
 - ⁵⁸ M. A. McGuire, A. D. Christianson, A. S. Sefat, B. C. Sales, M. D. Lumsden, R. Jin, E. A. Payzant, D. Mandrus,

- Y. Luan, V. Keppens, et al., Phys. Rev. B **78**, 094517 (2008).
- ⁵⁹ A. Akrap, J. J. Tu, L. J. Li, G. H. Cao, Z. A. Xu, and C. C. Homes, Phys. Rev. B **80**, 180502(R) (2009).
- ⁶⁰ S.-P. Kou, T. Li, and Z.-Y. Weng, Europhys. Lett. **88**, 17010 (2009).
- ⁶¹ J. Dai, Q. Si, J.-X. Zhu, and E. Abrahams, Proc. Nat. Acad. Sci. **106**, 4118 (2009).
- ⁶² J. van den Brink and D. Khomskii, Phys. Rev. Lett. **82**, 1016 (1999).
- ⁶³ J. van den Brink, G. Khaliullin, and D. Khomskii, Phys. Rev. Lett. **83**, 5118 (1999).
- ⁶⁴ J. van den Brink and D. Khomskii, Phys. Rev. B **63**, 140416(R) (2001).
- ⁶⁵ D. Senff, F. Krüger, S. Scheidl, M. Benomar, Y. Sidis, F. Demmel, and M. Braden, Phys. Rev. Lett. **96**, 257201 (2006).
- ⁶⁶ D. R. Neuber, M. Daghofer, A. M. Oleś, and W. von der Linden, Phys. Stat. Sol. (c) **3**, 32 (2006).
- ⁶⁷ A. M. Oleś, Phys. Rev. B **28**, 327 (1983).
- ⁶⁸ A. Moreo, M. Daghofer, J. A. Riera, and E. Dagotto, Phys. Rev. B **79**, 134502 (2009).
- ⁶⁹ E. L. Nagaev, Phys. Rev. B **58**, 827 (1998).
- ⁷⁰ D. I. Golosov, Phys. Rev. Lett. **84**, 3974 (2000).
- ⁷¹ N. Shannon and A. V. Chubukov, Phys. Rev. B **65**, 104418 (2002).
- ⁷² E. Bascones, M. J. Calderón, and B. Valenzuela, Phys. Rev. Lett. **104**, 227201 (2010).
- ⁷³ M. Daghofer, Q.-L. Luo, R. Yu, D. X. Yao, A. Moreo, and E. Dagotto, Phys. Rev. B **81**, 180514 (2010).
- ⁷⁴ C. C. Chen, J. Maciejko, A. P. Sorini, B. Moritz, R. R. P. Singh, and T. P. Devereaux (2010), arXiv:1004.4611.